Study of the influence of the artificial ageing temperature on the AA2024 alloy microstructure

Nicoleta Radutoiu[1,2], Joël Alexis[1], Loïc Lacroix[1,a], Marioara Abrudeanu[2], Jacques-Alain Petit[1]

[1] University of Toulouse, LGP-ENIT/INPT, 47 avenue d'Azereix, BP 1629, 65016 Tarbes, France
[2]University of Pitesti, Str. Targul din Vale, nr.1, 110040 Pitesti, Arges, Roumanie

[a]loic.lacroix@enit.fr

Keywords: over-ageing treatment, AA2024 aluminum alloy, microstructure, mechanical properties.

Abstract. For the last 30 years, AA2024 aluminum alloy was very used as structural material in the aerospace industry due to its low density and good mechanical strength. The phenomenon of precipitation hardening in aluminum alloys takes place at relatively low temperature and induces the precipitation of intermetallic particles composed of the main alloying elements i.e., copper and magnesium. The fundamental stage of the age-hardening process consists in the acceleration of the decomposition phenomenon of the supersaturated solid solution, resulting in the coarse intermetallic particle precipitation; stage where the mechanical properties reaches the maximum values, but at the cost of a low corrosion resistance. In this paper, the AA2024 alloy microstructure was studied during the over-ageing process. The over-ageing treatment (T7) is supposed to stabilize the microstructure and the mechanical properties to improve the corrosion resistance. The over-ageing treatment consists in a solution treatment at 495±5°C for 1 hour, quenched into cold water and artificial aged. Three different artificial ageing temperatures were studied: 150°C, 175°C and 190°C. The mechanical properties modifications were followed by Vickers macrohardness measurements. The treatment duration for each temperature (36 days for 150°C, 50 hrs for 175°C and 24 hrs for 190°C) was determined by a given macrohardness reduction.
To characterize the over-aged AA2024 alloy microstructure, a statistical analysis of the surface fraction and surface density of intermetallic particles was made. The intermetallic particle dimension distribution, depending on the over-ageing temperature, was also observed. To do so, scanning electron microscope observations were carried out and image analyses were performed from backscattered electron images.

Introduction

Aluminum alloys of the 2000 series are very used in aeronautical applications due to the high strength to weight ratio associated with good fracture toughness. Among these alloys, the AA2024 alloy possesses more than 40%, still making the most used material in the aircraft industry [1,2]. A combination of alloying elements, heat treatment and ageing induce improvement of mechanical properties, as well as good damage tolerance and resistance to fatigue [3,4,5]. On the contrary, the presence of copper and magnesium containing intermetallics, leads to susceptibility to localized corrosion [6,7,8,9]. The phenomenon of precipitation hardening and the influence of heat treatment on the mechanical properties of AA2024 alloy have been extensively studied [10,11]. The effects of natural and artificial ageing on the AA2024 alloy microstructure are relatively well known. The microstructure has an important role in corrosion resistance, and some intermetallic particles can be the cause of pitting and intergranular corrosion [12]. The complex decomposition sequence in the α+S phase field, is generally considered to be as follows: SSS→ zone GPB→ S"→ S'→S (Al_2CuMg) [4,13,14].
A complex microstructure consisting of many intermetallics is found after the thermomechanical treatment on the AA2024 alloy. There are hardening precipitates with a size of hundreds nanometers and coarse intermetallic precipitates with a size of some micrometers.

Two types of coarse intermetallic particles characterized the microstructure of AA2024 alloy. S-Al_2CuMg phase particles are small round particles of particular interest because they are reported to account for 60% of particles larger than 0,5 µm [6]. In contrast to the S-phase particles, the Al(Cu,Mn,Fe,Si) intermetallics present irregular shapes and size typically larger than 5 µm. In a study of the pitting corrosion on the AA2024 T3 alloy using "nuclear microprobe" analysis, Boag et al. [15] have confirmed the presence of intermetallic particles containing Al, Cu, Mn, Fe and Si with an average size of 20 µm, and S-phase particles smaller than previous ones. In addition, research conducted by Buchheit et al. [6] showed the presence of 61.3% of the S-phase particles, 12.3% of Al_6 (Cu,Fe,Mn), 5.2% of Al_7Cu_2Fe and 4.3% of $(Al,Cu)_6Mn$ in the AA2024 alloy .
The mechanical properties are improved due to hardening precipitation that lead to peak-ageing condition and to the over-ageing condition with increasing ageing. Corrosion damage of the material is also very essential to the structural integrity of the aircraft. In the literature [1] it is generally reported that the 2xxx wrought aluminum alloys in the T3 condition have low corrosion resistance compared to the T6 and T8 conditions.
In this paper, the AA2024 alloy microstructure was studied during the over-ageing process. To characterize the over-aged AA2024 alloy microstructure, a statistical analysis of the surface fraction and surface density of intermetallic particles were made. The intermetallic particle dimension distribution was also carefully studied as a function of the over-ageing temperature. The mechanical properties of the AA2024 alloy at the T351 state and over–ageing were studied locally (matrix and intermetallic particles) using nanoindentation at very low loads.

Experimental

The AA2024 alloy microstructure in terms of distribution and size of intermetallic particles was studied after the over-ageing process. The chemical composition of AA2024 alloy is shown in Table 1. All specimens were cut in order to test the longitudinal (L) direction of the material.

Table 1: Chemical composition (mass %) of the studied alloy

Chemical element	Al	Cu	Mg	Mn	Fe	Zn	Si	Ti	Cr
wt. %	Base	4.6	1.5	0.6	0.14	0.12	0.08	0.04	0.01

Table 2 shows the heat treatments performed on the samples. The sample with size of 1 cm^3, were treated at 495 ± 5°C in an air circulating furnace for 1 hour, quenched into cold water and immediately aged at three different temperatures: 150°C, 175°C and 190°C. The treatment duration for each temperature (36 days at 150°C, 50 hrs at 175°C and 24 hrs at 190°C) was defined after the macrohardness stabilized. Vickers hardness measurements were made with a load of 10 daN and 30 daN. The experimental values obtained for the two loads are almost similar.

Table 2: Heat treatments for the AA2024 alloy

Designated names for the heat treatments	Details
T351	Solution treated at 495±5°C, quenched, stretched 1.5-3%, aged at room temperature
T7-150	T351 + solution treated at 495±5°C for 60 min + water quenched, aged 36 days at 150°C

T7-175	T351 + solution treated at 495±5°C for 60 min + water quenched, aged 50 hrs at 175°C
T7-190	T351 + solution treated at 495±5°C for 60 min + water quenched, aged 24 hrs at 190°C

The method of surface preparation is important for the study of intermetallic particles. The surface preparation consisted of mechanical polishing from SiC paper (grade 600, 1000, 2500, 4000) to a diamond abrasive of 3 µm and 1 µm. Final polishing, 0.05 µm, is performed using a pure, heavy grade of silicon dioxide (SiO_2). The Vibromet polishing removes the deformation layer remaining after a classical mechanical preparation.
The evolution of the surface during polishing was followed by measurements of roughness (roughness arithmetic Ra, roughness total Rt), which were performed using the optical profiler Veeco NT 1100. The results are summarized in the Table 3.

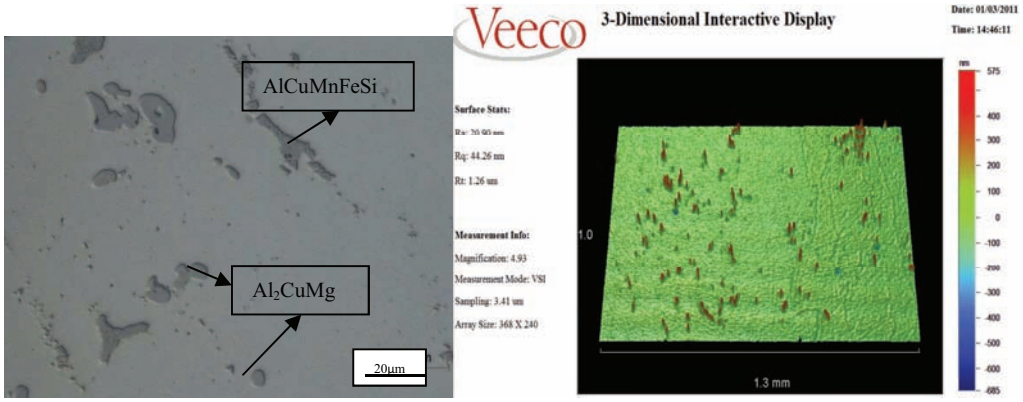

Figure 1: Optical analysis of the sample of the AA2024 alloy

Table 3: Roughness of the samples of the AA2024 alloy

	Ra (µm)	Rt (µm)
T351	0.025	1.30
T7-150	0.033	2.37
T7-175	0.298	2.46
T7-190	0.021	1.75

To characterize the over-aged AA2024 alloy microstructure scanning electron microscope (SEM) observations were carried out and image analyses were performed from backscattered electron images. The surface fraction and surface density is obtained by image analysis with the software Areas (Microvision).
Instrumented indentation has been widely used for determining the mechanical properties of material, respectively Young's modulus and hardness.
The mechanical properties of the matrix of the AA2024 alloy and its coarse intermetallic particles before and after thermical treatment were characterized using an MTS Nanoindenter with a Berkovich indenter tip. Heads XP and DCM were respectively used to characterize the matrix (solid solution and hardening precipitates) and coarse precipitates at depths up to 2000 nm and 300 nm.

Results and discussions

The artificial ageing leads to an improvement of the mechanical properties; the degree of precipitation hardening is a function of the temperature and treatment duration. The change in Vickers hardness, during artificial ageing can be drawn as a curve with a maximum value. Figure 2 presents the hardness variation as a function of the artificial ageing time for the three temperatures. So, the maximum hardness (peak hardness) at 150°C, 175°C and 190°C is reached respectively after 28 days, 11 hours and 7 hours of treatment, and a stabilization of the hardness appears respectively after 36 days, 50 hours and 24 hours. The maximum hardness is in agreement with the peak hardness found in literature [12,16,17]. The choice of the treatment duration was based on the stabilization of the hardness for each temperature.
The variation of hardness as a function of the artificial ageing time showed four stages that typically appear in the AA2024 alloy [5,16]:
- initial rapid hardness, characterized by an initial rapid hardening
- hardness plateau, indicating the stability of the hardness
- second hardness, characterized by an increase in hardness (peak hardness); has been attributed to the formation of the S' and S-phase
- over-ageing, hardness stabilization

The over-ageing treatment (T7) allows to stabilize the microstructure and to improve the corrosion resistance.

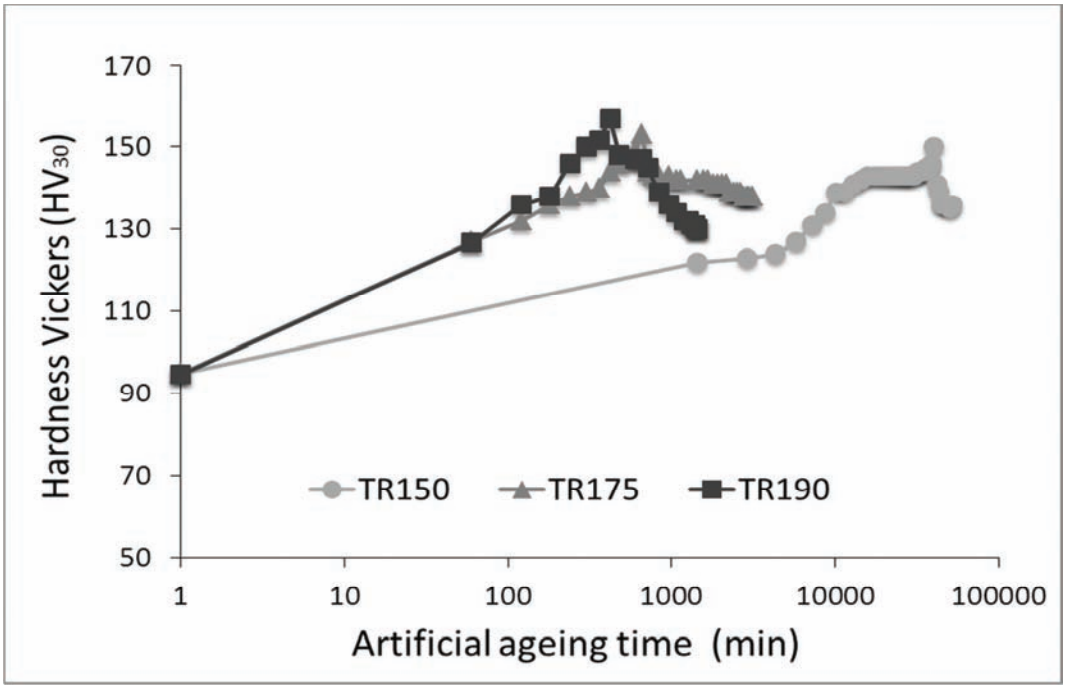

Figure 2: Hardness as a function of the artificial ageing time at 150°C, 175°C and 190°C

Distribution of the particles. The surface fraction (Fs) and surface density (Ds) of coarse intermetallic particles are given by the following equations (Eq.1 and Eq.2) where I.P. means intermetallic particles.

$$Fs = \frac{\text{Total area I.P.}}{\text{Total area analyzed}} \quad (1)$$

$$Ds = \frac{\text{Total number I.P.}}{\text{Total area analyzed}} \quad (2)$$

These parameters were determined from the analysis of backscattered electron SEM images. The methodology consisted of a statistical analysis of the surface fraction and chemical analysis of coarse intermetallic particles using image analysis and EDS analysis An optimal method was been developed from backscattered SEM micrographies. Figure 3 present this method starting from SEM images, followed by image analysis and finally data processing.

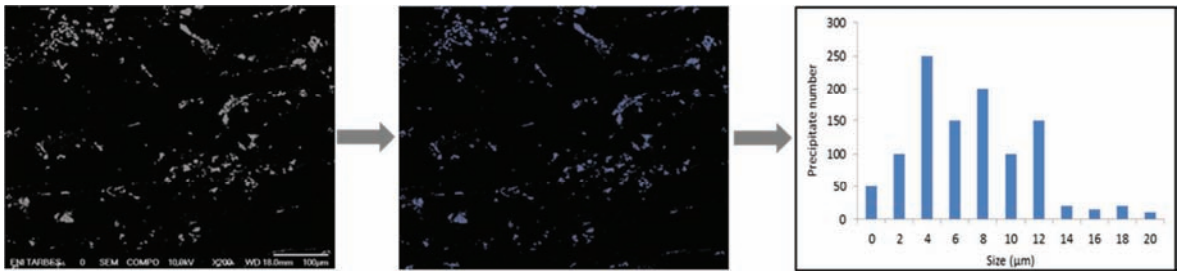

Figure 3: Methodology of statistical analysis from image analysis

The observations were made at three magnifications: X100, X200 and X400. The magnification X100 gives a value for the distribution of intermetallic particles, which stabilizes faster, but with a poor resolution. The magnification X400 gives scattered results making the study very time consuming to obtain a representative value for the surface distribution of coarse intermetallic particles from a large number of micrographies. The magnification X200 represents the best compromise; the representative value stabilizes after sufficient number of image analysis. In total, 21 SEM observations were analyzed, each micrography has an area of 0.29 mm^2; the total area analyzed for each sample is 6.01 mm^2. Figure 4 shows the surface fraction of the coarse intermetallic particles in the over-aged conditions as a function of the analyzed area for a X200 magnification for different metallurgical state. It is observed that the minimum area to be analyzed to obtain representative values is about 4 mm^2. It is observed a slight decrease in the surface fraction with the over-ageing temperature. This variation can be associated with the temperature dependence of the solubility and the diffusion rate.

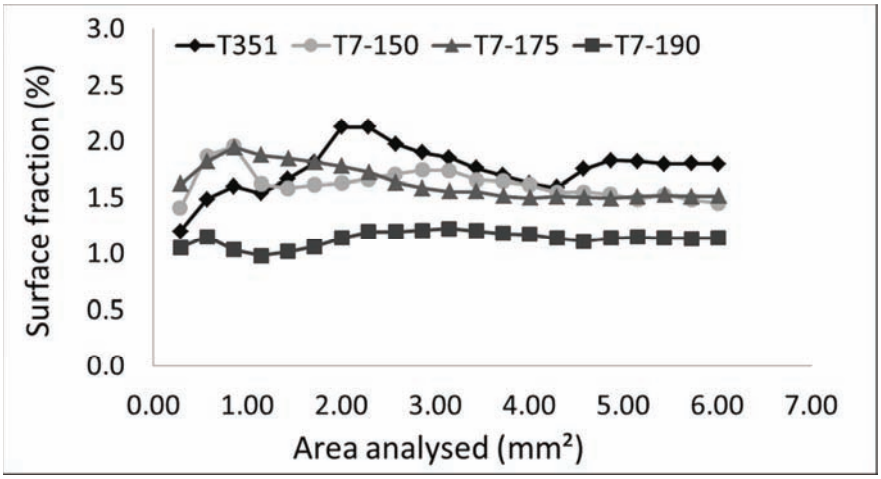

Figure 4: Surface fraction as a function of the analyzed area

In Table 4 are presented the results of the surface fraction and surface density. The values are slightly lower comparing with the values obtained by Buchheit and al [6]. They found a surface fraction of 2.69% for the S-phase. It should be mentioned, that in this study the surface fraction (Fs) includes the S-phase (Al_2CuMg) and Al(Cu,Mn,Fe,Si) particles. Moreover, only the particles with size greater than 2 µm were detected.

Table 4: Results in the evolution of intermetallic particles

	T351	T7-150	T7-175	T7-190
Fs (%)	1.8 ± 0.19	1.5 ± 0.09	1.5 ± 0.12	1.1 ± 0.05
Ds (particles/mm^2)	457 ± 24	377 ± 15	675 ± 50	577 ± 36

Classification of intermetallic particles. This study was conducted to analyze the coarse intermetallic particles by chemical composition and size (equivalent diameter). The chemical composition of the particles was obtained by electron dispersive spectrometry (EDS) analyses. Hence, EDS analyses was used to sort particles into major categories by alloying elements detected and by relative concentration of those elements.
EDS showed two major types of intermetallic particles. A first group of particles containing Al, Cu and Mg exclusively, this class represents the Al_2CuMg particles, so called S-phase [6]. Figure 5 shows such a particle with a spectral analysis.

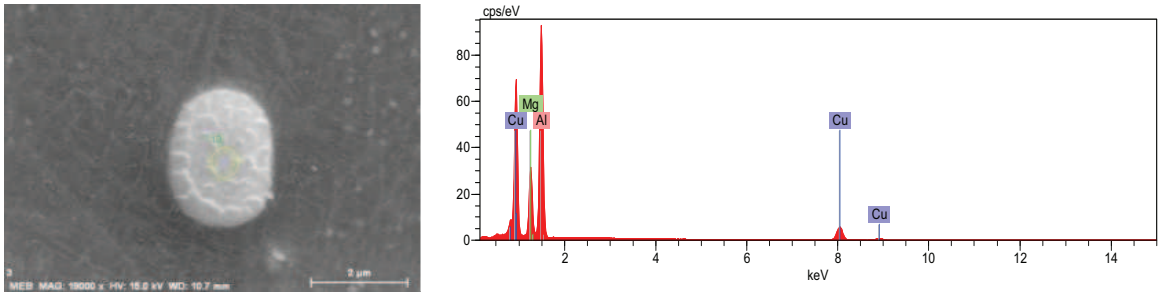

Figure 5: SEM micrography of an S-phase particle and the associated EDS analysis

The chemical composition was calculated for a certain number of the Al_2CuMg particles and the average value is presented in the table 5. Calculated chemical composition is practically identical with the stoichiometric composition (Al-50 %at, Cu-25 %at, Mg-25 %at).

Table 5: Chemical composition of the Al_2CuMg particles

	Al (at.%)	Cu (at.%)	Mg (at.%)
T7-150	52.8	24.6	22.5
T7-175	50.3	25.4	24.1
T7-190	52.9	24.2	22.7
Stoichiometric composition S Phase -Al_2CuMg	50	25	25

The second group detected is Al(Cu,Mn,Fe,Si) particles [10]. In the literature it exists many different phases, depending on the chemical composition: Al_8Fe_2Si, $Al_{10}Mn_3Si$ [18], Al_7Fe_2Cu, $Al(Cu)_6Mn$ [19]. Figure 6 shows a SEM micrography of a Al(Cu,Fe,Mn,Si) particle and the associated EDS spectrum. The table 6 presents the average values calculated from chemical composition.

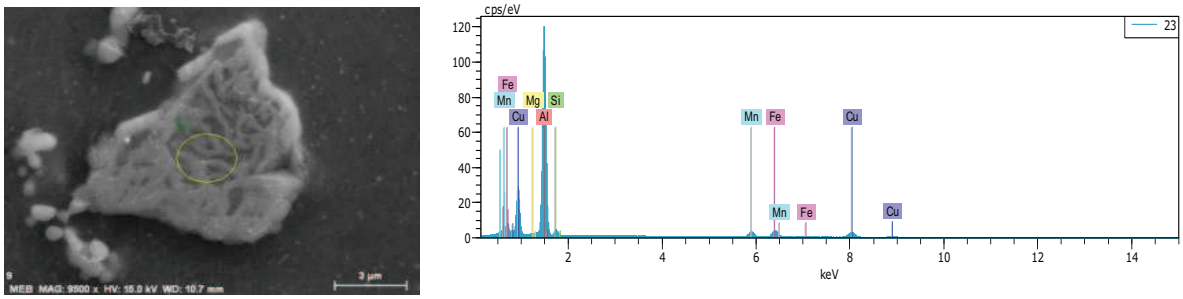

Figure 6: SEM micrography of an Al(Cu,Mn,Fe,Si) particle and the associated EDS analysis

Table 6: Chemical composition of the Al(Cu,Mn,Fe,Si) particles

	Al (at.%)	Cu (at.%)	Fe (at.%)	Mn (at.%)	Si (at.%)	Mg (at.%)
T7-150	71.5	16.3	6.0	4.0	1.1	0.8
T7-175	71.9	15.0	5.9	4.5	1.2	0.9
T7-190	71.6	15.8	6.0	4.3	1.2	0.9

A statistical analysis of the intermetallic particles dimension distribution was realized. Image analysis has been performed on the intermetallic particles to characterize the evolution of the equivalent diameter. Figure 7 shows the distributions of the equivalent diameter. At the ageing condition T7-175 and T7-190, the majority of intermetallic particles (70%) have the equivalent diameter between 2-6 µm, and at the ageing condition T351 and T7-150 the proportion of intermetallic particles with the equivalent diameter between 2-6 µm, is somewhat lower (50%). The majority of the particles that forms after a heat treatment are S-phase particles.

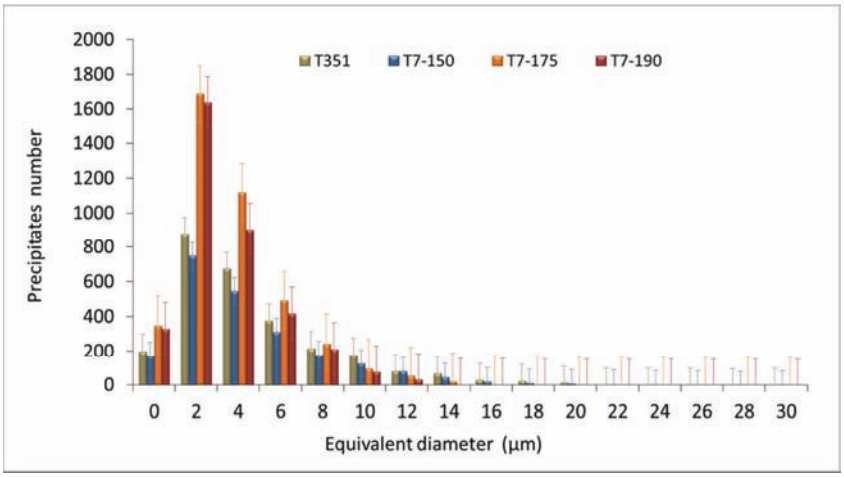

Figure 7: Distribution of the intermetallic particles as a function of the equivalent diameter

Nanoindentation test. Nanoindentation has been used to determine the mechanical properties of the matrix of the AA2024 alloy for the different ageing condition, and particularly to determine the mechanical properties of coarse intermetallic particles. One of the most used methods for analyzing the mechanical properties is that of Oliver-Pharr [20,21]. Nanoindentation tests in dynamic mode (Continuous Stiffness Measurement) are achieved in the matrix and the coarse precipitates at a maximum depth of respectively 2000 nm and 300 nm. The low maximum depth for the coarse precipitates was defined taking into account not only their small size but also errors induced by the roughness.

In Figure 8 and 9 are presented the load-displacement curves for the AA2024-T351 alloy and the over-aged AA2024 alloy, respectively the load displacement curves for the matrix, the S-phase (Al_2CuMg) and the Al(Cu,Mn,Fe,Si) particles of the alloy AA2024 T7-150.
From loading – unloading curves, the mechanical behavior is determined by calculating the ratio of plastic deformation work and the elastic deformation work. This ratio increases slightly after quenching.

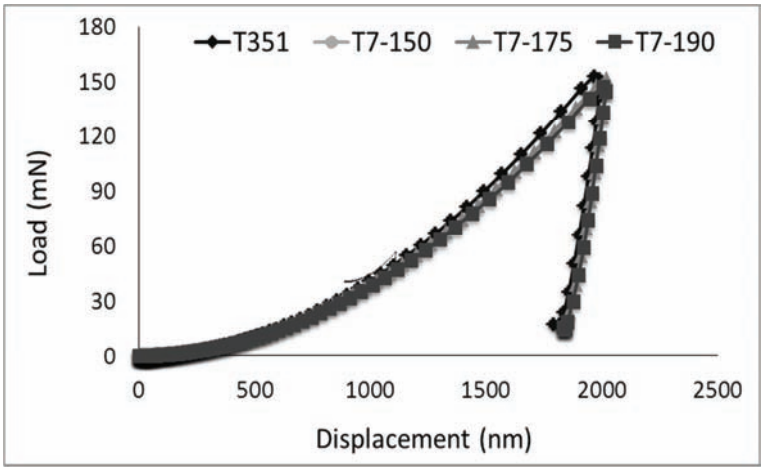

Figure 8: Load –displacement for the AA2024-T351 and AA2024 over-ageing

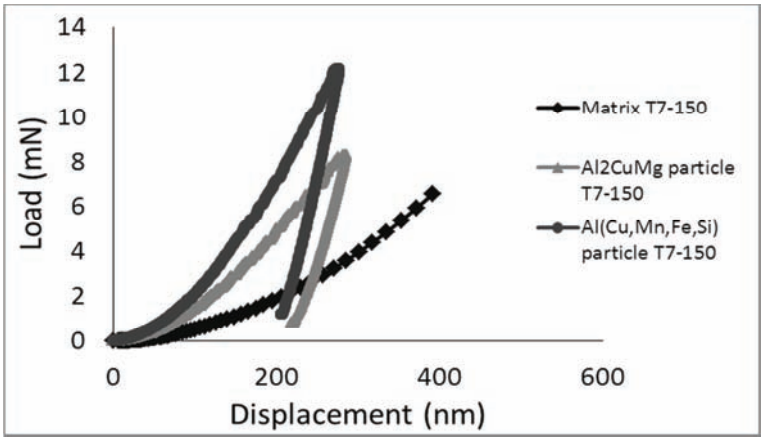

Figure 9: Load - displacement for the matrix, the Al_2CuMg and the Al(Cu,Mn,Fe,Si) particles of the AA2024 T7-150 alloy.

The mechanical properties of the materials depend on their microstructure. It depends on the presence of intermetallic precipitates and their surface repartition. These mechanical characteristics were determined for indentation depths between 150 and 1800 nm. The mechanical properties of the matrix (solid solution and hardening precipitates) appear identical for the three treatment conditions chosen. Young's modulus is close to 85 GPa and the hardness is equal to 1.7 GPa.
A distribution of intermetallic particles was performed according to the hardness and Young's modulus. We can see that, in Figure 10, in case of the coarse intermetallic precipitate the values of the mechanical properties are not homogeneous; Young's modulus varies between 110-190 GPa and hardness between 6-12 GPa.

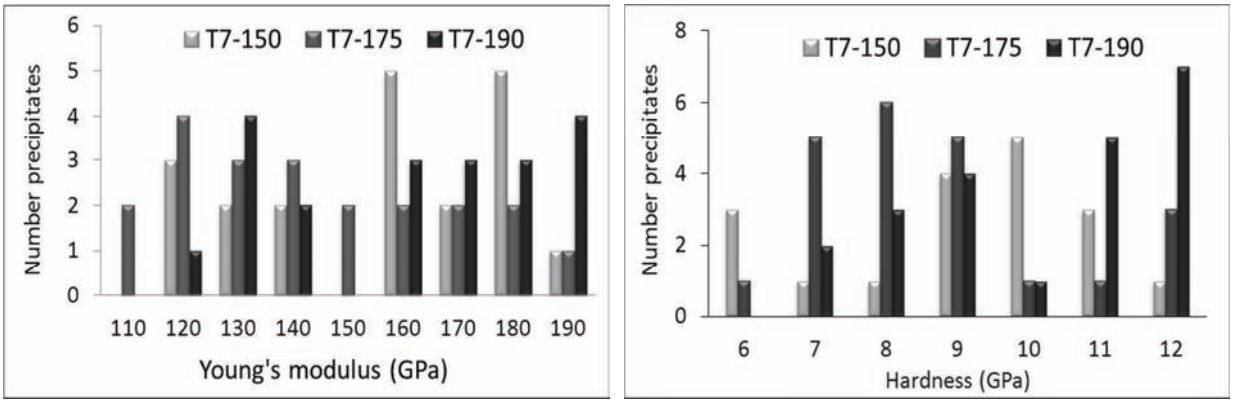

Figure 10: Distribution of intermetallic particles as a function of mechanical properties

The hardness values measured by nanoindentation exhibit the same tendency as for the Vickers measurements (136 HV_{30} for T7-150, 139 HV_{30} for T7-175, 133 HV_{30} for T7-190). The Young's modulus and hardness are presented in Table 7.

Table 7: Mechanical properties data for the matrix AA2024-T351 and AA2024 aged alloy

Matrix			
	Young's Modulus (GPa)	Hardness (GPa)	W_P/W_e
T351	84.4 ± 0.1	1.9 ± 0.1	3.7
T7-150	87.0 ± 1.9	1.7 ± 0.1	3.9
T7-175	85.6 ± 0.1	1.8 ± 0.1	3.9
T7-190	84.9 ± 1.1	1.7 ± 0.1	3.9

In order to determine the mechanical properties of coarse intermetallic particles the nanoindentation tests were performed on 50 precipitates in each aging condition. The precipitates in which indentations were performed were analyzed by EDS to determine their chemical composition. Figure 11 shows the SEM images of the nanoindented shapes obtained through nanoindentation of the S-phase (Al_2CuMg) and the Al(Cu,Mn,Fe) particles.

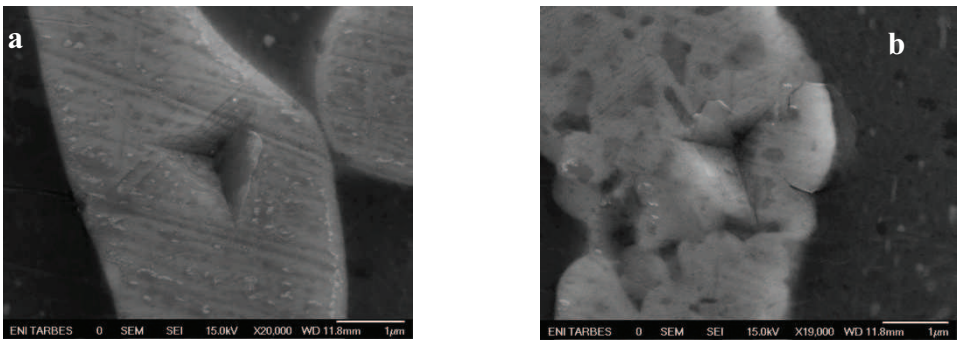

Figure 11: SEM images after nanoindentation of the Al_2CuMg particles (a) and Al(Cu,Mn,Fe) particles (b)

We determined Young's modulus and hardness values for the S-phase particles and the Al(Cu,Mn,Fe,Si) particles. The results for each condition were presented in Table 8. It can be noted that S-phase particles present Young's modulus and hardness values lower than the Al(Cu,Mn,Fe,Si) particles.

Table 8: Mechanical properties of coarse intermetallic particles

Intermetallic particles				
	Al_2CuMg		Al(Cu,Mn,Fe,Si)	
	Young's Modulus (GPa)	Hardness (GPa)	Young's Modulus (GPa)	Hardness (GPa)
T7-150	131.1 ± 3.9	6.4 ± 0.5	173.7 ± 14.5	9.5 ± 1.1
T7-175	132.7 ± 7.8	7.2 ± 0.8	174.7 ± 17.4	9.5 ± 1.8
T7-190	139.9 ± 3.5	7.5 ± 0.6	179.3 ± 15.6	10.2 ± 1.3

Conclusions

1. The SEM observations and EDS analyses confirmed presence of two types of coarse intermetallic particles: Al_2Cu Mg and Al(Cu,Mn,Fe,Si).
2. Vickers hardness of the over-aged AA2024 alloy are lower than the AA2024-T351 alloy (136 HV_{30} for the over-aged AA2024 and 149HV_{30} for AA2024-T351 alloy). At the same time, the treatment duration has been determined for each temperature (36 days for 150°C, 50 hours for 175°C and 24 hours for 190°C). For these durations of the over-aging treatment, the hardness is almost identical (136 HV_{30}, 139 HV_{30} and 133 HV_{30} respectively for over-ageing treatment at 150°C, 175°C and 190°C).
3. The nanoindentation tests have confirmed similar hardness and Young's modulus values of the matrix (solid solution and hardening precipitates) for the different over-ageing treatments. The mean values calculated for the different treatment are close to 85 GPa for the Young's modulus and 1.7 GPa for the hardness.
4. Rigidity and hardness of the intermetallic particles are higher than those of the matrix. The hardness values and Young's modulus values of the Al(Cu,Mn,Fe,Si) phases are higher than those of the S-phase.

Acknowledgement
This article was produced under the project "Supporting young PhD Student with frequency by providing doctoral fellowships" – ID 52826 co-financed from the European Social Fund, through the Sectorial Operational Program Development of Human Resources.

References

[1] D. N. Alexopoulus, Mater. Sci. Eng. A50 (2009), p. 40
[2] A. May, M.A. Belouchrani, S. Taharboucht and A. Boudras, Proc. Eng. 2 (2010), p.1795
[3] K.S. Al-Rubaie, M.A. Del Grande, D.N Travessa and K.R Cardoso, Mater. Sci. Eng. A 464(2007), p.141
[4] S. Wang and M. Starink, Acta Mater. 55 (2007), p.933
[5] S. P. Ringer and K. Hono, Mater. Character. 44 (2000), p.101
[6] R. Buchheit, R. Grant, P. Hlava, B. McKenzie and G. Zender, J. Electrochem. Soc. 144 (1997), p.2621
[7] M. B. Vukmirovic, N. Dimitrov and K. Sieradzki, J. Electrochem. Soc. 149 (2002), p.428
[8] C. Blanc, S. Gastaud and G. Mankowski, J. Electrochem. Soc. 150 (2003), p.396
[9] L. Lacroix, L. Ressier, C. Blanc, and G. Mankowski, J. Electrochem. Soc. 155 (2008), p.8
[10] A.K. Mukhopadhyay, Met. Mater. and Process. 19 (2007), p.1
[11] S.C. Wang and M. J. Starink, Int. Mater. 50 (2005)p.193

[12] J.R. Davis (eds.), ASM Specialty Handbook: Aluminum and Aluminum Alloys, ASM International, Metals Park, OH, USA, (1993)
[13] J.M. Silckok, J. Inst. Met. 88 (1960), p.357
[14] I.N. Khan, M. J. Starink and J. L. Yan, Acta Met. Eng. A 472 (2008), p.66
[15] A. Boag, D. McCulloch, D. Jamienson, S. Hearne, A. Hughes, C. Ryan and S. Toh: Nuclear Instruments and Methods in Physics Research Section B: Beam Interactions with Materials and Atoms 231(1-4) (2005), p. 457
[16] R. Develay, Techniques de l'Ingénieur, Paris, France, MD2 M1290, (1986)
[17] M. Massazza and G. Riontino, Phil. Mag. Lett. 82 (9) (2002), p. 495
[18] R. Wei, C.-M. Liao and M. Gao, Metal. Mat. Trans. A 29(4) (1998), p.1153
[19] V. Guillaumin and G. Mankowski, Corros. Sci. 41 (1999), p.421
[20] W.C. Oliver and G.M. Pharr, J. Mater. Res. 7 (1992), p.1564
[21] M.K. Khan, S.V. Hainsworth, M. E. Fitzpatrick and L. Edwards, J. Mater. Sci. 44 (2009), p.1006